Modeling of the compression of coated papers in a soft rolling nip

V. Litvinov · R. Farnood

Abstract An analytical model is developed for the compression of coated substrates in a soft rolling nip formed between a hard roll and a soft covered roll. The coating layer, substrate, and soft cover are modeled as a stack of three layers that are compressed jointly while passing through the nip. Material models have been adopted separately for each of the three layers and were combined together according to the thickness of individual layers. In this study, the substrate is considered to be a viscoelastic–plastic material and is represented by a modified solid element while the coating layer is assumed to be elastic and the soft cover material is approximated by a standard Maxwell model. A strain function is derived for the compression of substrate in the nip that appears to be a parabolic function of time. Substrate compression in the nip and its subsequent relaxation are calculated by solving a set of differential equations that describe the coating, substrate, and soft cover deformations. This model is used to study the soft-nip calendering of coated papers. Examples of numerical modeling that demonstrate the paper deformation and stress profiles in the nip are presented. In addition, the effects of paper and cover properties as well as calendering parameters on the dynamics of paper compression are discussed. Finally, a comparison of the modeling results is made with the experimental data.

V. Litvinov · R. Farnood (✉)
Department of Chemical Engineering and Applied Chemistry,
University of Toronto, Toronto, ON, Canada
e-mail: ramin.farnood@utoronto.ca

Present Address:
V. Litvinov
Forming Technologies Inc, Oakville, ON L6M 2G2, Canada

Introduction

Commercial production and applications of coated substrates may involve compression of such materials between two rolling cylinders to achieve the desired surface finish and performance. An example of such a process is the calendering of coated paper. In particular, calendering of coated writing and printing papers enhances their appearance and printability by improving surface smoothness and gloss. At the same time, calendering decreases paper thickness and thickness variations, porosity, and air permeability by the bulk compression of the paper structure. Therefore, modeling of coated paper compression is important not only for the fundamental understanding of paper's response to calendering, but also as a practical tool for product development, quality improvement, equipment design, and on-line control.

Compressive behavior of paper has been studied intensively in the literature and various theoretical models have been developed to describe this process. These models can be classified into four main categories: material models, empirical models, finite element analysis, and network modeling. In material models, the stress and strain behavior of the material is represented by simplified analytical expressions [5, 8, 10, 19, 25, 26]. On the other hand, empirical models derived from pilot and commercial data have been widely accepted and utilized in the hard-nip calendering of paper [4, 6, 19], while their extension to the soft-nip calendering process [9] has found limited application due to the complex cover–paper interactions and the wide range of soft cover material properties. In recent years, finite element analysis [22, 24, 31] has been used intensively for the modeling of hard-nip and soft-nip calendering of uncoated papers. This method relies on the continuum assumption, as well as the discretization of paper and soft cover to a large number of finite elements.

However, if using this method, one must still choose an appropriate constitutive model for paper. Finally, in the network modeling approach, paper is represented as a random assembly of fibers. Fiber characteristics and paper structure affect the compressive response of paper [27], and in principle, paper's compressive behavior can be estimated from these two parameters. The idea of the network model has been discussed by various researchers in recent years [13, 17, 20, 21]. In particular, using dynamic finite element modeling, Kwong and Farnood [13] studied the effect of fiber characteristics on the compression of a three-dimensional fiber network, representing paper. Predictions of their model qualitatively and quantitatively agreed with the experimental data.

The key difference between hard-nip and soft-nip calendering is the time of contact between paper and the calender rolls; or, equivalently, the nip length. In the soft-nip calendering, one of the rolls is covered by a relatively "soft" polymeric material. The elastic modulus of the soft cover material for paper calendering is in the range of 1–10 GPa [18], whereas hard rolls are typically made of steel with a modulus of elasticity of about 200 GPa. This leads to a rather large deformation of soft cover in the nip and consequently an increase in the nip length, a higher dwell time, and a lower average compressive stress in the substrate. Calendering of coated papers involves the added complexity of the simultaneous deformation of coating layer, paper substrate, and soft cover.

In our earlier articles, we have reported phenomenological and numerical models to predict the compression of uncoated papers and free coating layers [1, 2, 13, 14]. The aim of this study is to develop a material model for the compression of coated substrates in a soft rolling nip and apply this model to study the soft-nip calendering of coated papers.

Theory

Single stack element model

Earlier works have shown that the compression of coated paper in the calender nip is essentially a one-dimensional process [3]. Therefore, soft-nip calendering of coated papers can be simply modeled as the compression of a multilayer film between rolling hard cylinders. The substrate, the coating layer, and the soft cover are compressed and deformed simultaneously against rigid hard rolls (Fig. 1). In this work, this multilayer body is referred to as the "stack," and is modeled as a serial assembly of three one-dimensional elements.

In this study, the motion and deformation of a coated substrate are represented by the translational movement
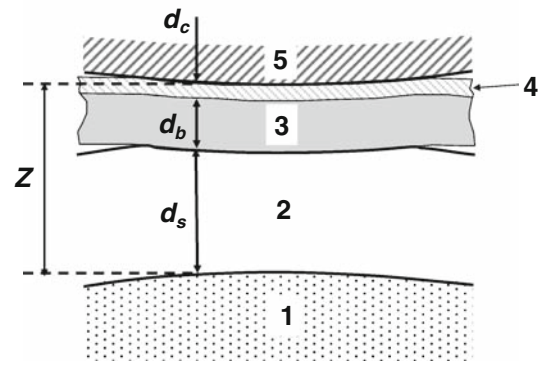

Fig. 1 Schematic diagram of compression of a coated substrate in a soft rolling nip: (1) covered roll; (2) soft cover; (3) substrate; (4) coating layer, and; (5) hard roll. The total stack thickness, Z, is sum of the substrate thickness, d_b, the coating thickness, d_c, and the soft cover thickness, d_s

and the traverse compression of each stack element. However, the lateral interaction of neighboring elements during the calendering process is ignored. Furthermore, the plane strain condition is assumed: this implies negligible strain variations under the nip in the cross-machine direction. These assumptions simplify the mathematical treatment of soft-nip calendering.

Starting with the compatibility relationship, the total deformation of the stack element (ΔZ) is:

$$\Delta Z = \Delta d_s + \Delta d_p \tag{1}$$

where d_s is the soft cover thickness, and d_p is the total thickness of coated substrate, that in turn is expressed as the sum of the substrate thickness (d_b) and the coating thickness (d_c). The deflection of each layer can be expressed by:

$$\Delta Z = \varepsilon Z_o \tag{2a}$$

$$\Delta d_i = \varepsilon_i d_{oi} \tag{2b}$$

where ε and ε_i represent the engineering strains in the stack and in the layer "i", respectively; and subscript "o" indicates the initial thickness of each layer prior to the deformation in the nip.

The initial thickness of coated substrate can be expressed as a fraction (α) of the total stack thickness: $d_{op} = \alpha Z_o$. Similarly, the initial coating thickness can be described as a fraction (β) of the total thickness of coated substrate: $d_{oc} = \beta d_{op}$. Therefore, by combining Eqs. 1 and 2:

$$\varepsilon = \alpha \varepsilon_p + (1 - \alpha)\varepsilon_s \tag{3a}$$

$$\varepsilon_p = \beta \varepsilon_c + (1 - \beta)\varepsilon_b \tag{3b}$$

$$\varepsilon = \alpha \beta \varepsilon_c + \alpha(1 - \beta)\varepsilon_b + (1 - \alpha)\varepsilon_s \tag{3c}$$

Equation 3c allows us to combine the compressive behavior of the soft cover, the substrate, and the coating layers.

In the case of soft-nip calendering of coated paper, thickness values for the soft cover, coated paper, and coating layer are of the order of 10, 0.1, and 0.01 mm, respectively. Therefore, $\alpha \ll 1$ and $\beta \ll 1$.

Strain profile

The strain on the stack element depends on the properties of the substrate and soft cover material, calender geometry, applied load, and the linear speed of the coated substrate. However, the strain distribution under the nip can be approximated based on the geometry of the calender rolls and the maximum level of stack compression in the nip.

Here, the mechanical model of stack compression is built as a kinematic actuation where the upper end-point of the stack element moves along the circular segment defined by the intersection of the stack and hard roll surfaces (Fig. 2). The instantaneous position of the stack element is represented by its location along the x-coordinate or by the corresponding time, $t = x/v$, where "v" is the linear speed of substrate. Using these notations, the position of stack element can be defined by the dimensionless time, $\tau = t/t_1 = x/a$, where "a" is the ingoing nip width and t_1 is equal to a/v. The dimensionless time when the coated substrate enters the nip is equal to '−1' and reaches zero at the point of maximum geometrical compression. τ continues to increase until the coated substrate leaves the nip, but it remains smaller than unity since the outgoing nip is shorter than the ingoing nip.

Based on the roll geometry and the maximum compression of the stack element (ε_{max}), the stack strain (ε) can be obtained as a function of the dimensionless time (see Appendix 1):

$$\varepsilon = \varepsilon_{max}(1 - \tau^2). \tag{4}$$

In reality, the maximum strain of the stack element depends on the applied load and the stack properties. However, for a given nip geometry, this parameter can be calculated from:

$$a = \sqrt{2r\varepsilon_{max}Z_0}, \tag{5}$$

where r is the equivalent roll radius and is defined as $1/r = 1/r_1 + 1/r_2$. In this equation, r_1 and r_2 are the radii of hard roll and soft roll, respectively (Fig. 2).

Although the exact nip width and strain profile depend on the Poisson ratio of the soft cover material [4, 7], Equation 4 provides a simple approximation of the nip geometry.

Substrate deformation

In this study, the substrate is represented by a modified standard solid element model composed of a nonlinear spring and a nonlinear Kelvin-like component as in Fig. 3 [8, 14]. The elastic modulus of nonlinear spring (E_o) is considered to increase with the applied stress according to:

$$E_0 = E_i + N_i\sigma(t), \tag{6}$$

where $\sigma(t)$ is the absolute value of the compressive stress, and E_i and N_i are constants. Equation 6 reflects an increase in the elastic modulus of substrate with an increase in the compressive stress. This is a reasonable assumption for porous substrates such as paper since higher stress levels result in increased densification and stiffness.

The Kelvin-like component includes a nonlinear element of dry friction (E_2) that is responsible for the irreversible plastic deformation of substrate. E_2 behaves
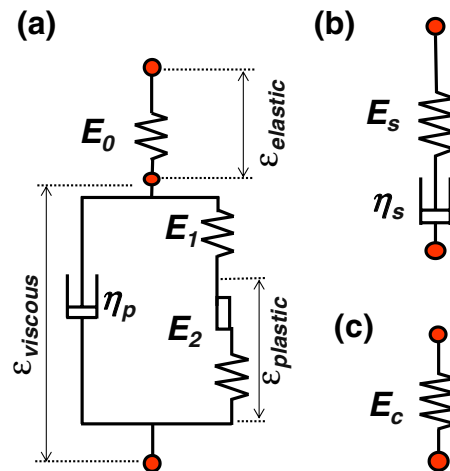

Fig. 2 Geometrical representation of stack deformation in a soft rolling nip

Fig. 3 Material models used for **a** substrate, **b** soft cover, and **c** coating layer

similar to a spring during the compression stage and stores the deformation during the unloading stage:

$$\varepsilon_{\text{plastic}} = \{\sigma_{K,\text{plastic}}(t)/E_2, \ t < t_{\text{p}};$$
$$\sigma_{K,\text{plastic}}(t_{\text{p}})/E_2, \ t \geq t_{\text{p}}\}, \tag{7}$$

where $\sigma_{K,\text{plastic}}$ is stress in the element of dry friction, and t_{p} corresponds to the time required to achieve the maximum strain of the Kelvin-like component. Furthermore, the total stress in the Kelvin-like component is:

$$\sigma(t) = \sigma_{K,\text{viscous}}(t) + \sigma_{K,\text{plastic}}(t), \tag{8}$$

where $\sigma_{K,\text{viscous}}$ is the stress in the dashpot.

Since the viscous and elastic strains in the Kelvin-like component are equal, the irreversible plastic deformation can be calculated from:

$$\varepsilon_{\text{plastic}} = \frac{E_{12}}{E_2}\varepsilon_{\text{viscous}}(t_{\text{p}}), \tag{9}$$

where E_{12} is the equivalent elastic modulus given by $E_1E_2/(E_1 + E_2)$.

Therefore, the set of equations that describe the deformation of the substrate during the loading stage are:

$$\varepsilon_{\text{b}}(t) = \varepsilon_{\text{elastic}}(t) + \varepsilon_{\text{viscous}}(t) \tag{10a}$$

$$\sigma(t) = E_{12}\varepsilon_{\text{viscous}}(t) + \eta_{\text{p}}\varepsilon'_{\text{viscous}}(t) \tag{10b}$$

$$\sigma(t) = (E_i + N_i\sigma(t))\varepsilon_{\text{elastic}}(t). \tag{10c}$$

Here, the viscosity of the substrate is denoted by η_{p}. The boundary conditions are defined at the point of first contact:

$$\varepsilon_{\text{b}}(-t_1) = \varepsilon_{\text{elastic}}(-t_1) = \varepsilon_{\text{viscous}}(-t_1) = 0 \quad \text{and}$$
$$\sigma(-t_1) = 0. \tag{10d}$$

For the unloading stage, the plastic strain remains unchanged and Eq. 10b should be replaced by:

$$\sigma(t) = E_1(\varepsilon_{\text{viscous}}(t) - \varepsilon_{\text{plastic}}(t_{\text{p}})) + \eta_{\text{p}}\varepsilon'_{\text{viscous}}(t), \tag{10e}$$

where $\varepsilon_{\text{plastic}}(t_{\text{p}})$ represents the residual plastic deformation of the dry friction element.

By combining Eqs. 4 and 10, the differential equation for the plastic strain of substrate is obtained:

$$T_{\text{p}}\varepsilon'_{\text{viscous}}(t) + \varepsilon_{\text{viscous}}(t)$$
$$= \frac{E_i}{N_iE_{12}}\left(\frac{1}{1 + N_i(\varepsilon_{\text{viscous}}(t) - \varepsilon(t))} - 1\right), \tag{11}$$

where $T_{\text{p}} = \eta_{\text{p}}/E_{12}$ is the characteristic time constant of substrate that can be determined from experimental data. Differential equations for the total, elastic, and viscous strains, as well as the stress in the substrate, can be obtained in a similar fashion.

Coating layer deformation

In this study, the coating layer is represented by an elastic element. This is a reasonable approximation since: (1) the thickness of coating layer is typically an order(s) of magnitude smaller than that of substrate, and; (2) for coated papers, experimental evidence indicates that the elastic modulus of the coating layer is about one order of magnitude larger than that of the paper substrate [30]. Therefore, any permanent deformation of the coating layer compared to that of substrate is negligible, and the coating layer could be simply modeled using Eq. 12 (Fig. 3):

$$\sigma(t) = E_{\text{c}}\varepsilon_{\text{c}}(t), \tag{12}$$

where E_{c} is the elastic modulus of coating layer.

Soft cover deformation

During the calendering process, the soft cover is repeatedly subjected to a short-duration (<1 ms) small-amplitude (<0.01 m/m) strain pulse. Experiments by Vuoristo et al. [28, 29] show that under these conditions soft cover materials exhibit viscoelastic characteristics with a time constant (T_{s}) of 10–20 ms. This time constant is sufficiently small to allow for strain relaxation between two consecutive pulses in a typical calendering operation.

In this study, the standard Maxwell model is used to describe the viscoelastic behavior of soft cover in the calendering nip (Fig. 3). The differential equation and the boundary condition for this model are given by:

$$E_{\text{s}}\varepsilon'_{\text{s}}(t) = \sigma'(t) + \frac{E_{\text{s}}}{\eta_{\text{s}}}\sigma(t) \tag{13a}$$

$$\varepsilon_{\text{s}}(-t_1) = 0 \tag{13b}$$

Once the stress history in the stack element is determined, the soft cover strain (ε_{s}) can be calculated from the above equation.

Deformation of the stack element

In order to find the stress history in the stack element, Eqs. 3(a–c), 11–13(a, b) have to be solved simultaneously. However, since the substrate, soft cover, and coating layer experience identical instantaneous stress levels, the strain functions for these layers can be determined independently. An example of this approach for uncoated substrates can be found in Appendix 2.

Based on this methodology, nonlinear differential equations that describe the viscoelastic–plastic deformation of the stack have been obtained and solved by numerical integration. The resulting stress profile was used to calculate the applied load on substrate:

$$L = \int_s \sigma \, \mathrm{d}x = -v \int_{-t_1}^{t_2} \sigma(t)\mathrm{d}t, \tag{14}$$

where L is known as the "line load," and t_1 and t_2 correspond to the times of entrance and exit of the coated substrate to and from the nip.

Results and discussion

Using the above theoretical model, a parametric study of the soft-nip calendering of coated papers in terms of the operating conditions and properties of paper and soft cover is conducted. The range of calendering variables and the adopted reference values are summarized in Table 1. Unless stated otherwise, these reference values are used in the parametric study.

Paper was described by a set of five parameters, as given in Table 2. These values were determined by curve-fitting of the stress–strain data reported by Rodal [23] for a bleached sulphite paper at low (paper #1) and high (paper #2) calendering temperatures. The total paper thickness and the thickness of coating layer prior to the calendering were maintained at 127 and 12.7 μm, respectively, throughout this study.

The soft cover's viscosity (η_s) was estimated based on its time constant (T_S) and modulus of elasticity (E_s) from $\eta_s = T_s E_s$. The time constant was chosen such that it allows for strain relaxation between two consecutive nip impressions, and E_s was taken from published hardness data [18, 29].

Table 1 The range of parameters and the adopted reference values in this study

Parameter	Range	Adopted value
Line load (kN/m)	0–350	250
Paper speed (m/min)	300–2500	1200
Roll diameter (mm)	350–1100	600
Cover thickness (mm)	0–130	12.7
Cover elasticity (GPa)	1.5–6	6
Cover viscosity (KPa s)	10–20	20
Coating elasticity (GPa)	0.1–5	1

Table 2 Model parameters for base paper in this study

	Paper #1	Paper #2
Temperature (°C)	23	107
E_i (MPa)	8	90
N_i	4	5
E_1 (MPa)	20	20
E_2 (MPa)	5	5
η_p (MPa s)	0.04	0.03

Maximum stress and stress profile

The estimated maximum stress for typical ranges of commercial printing papers is found to be practically independent of their viscoelastic parameters. Figure 4 illustrates the effect of applied line load on the predicted maximum and average stresses for papers #1 and #2. Based on this figure, the maximum stress values for these papers at a line load of 100 KN/m is about 20 MPa; that is, of the same order of peak pressure measured elsewhere [15]. For comparison, the static stresses according to the Hertz theory are also plotted in this graph. Hertz's solution describes the frictionless contact of two perfectly smooth isotropic elastic cylinders under the normal compressive load; consequently, it does not take into account the presence of coated paper in the rolling nip. This simplification leads to errors in the determination of the deformation profile in the contact zone as well as in the magnitudes and the distribution of stress and strain. In addition, Hertz's solution is valid for a purely elastic contact problem and does not account for viscous deformation in the soft cover and for the viscoplastic deformation of paper. Nevertheless, the level of inaccuracy is generally assumed to be small, and in the absence of other theoretical solutions for the contact problem, Hertz's theory is widely used as a common comparison standard. However, a close examination of Fig. 4 shows that, in this case, the stress values predicted from the Hertz theory are about twice as large than those calculated from the present model. This is consistent with the findings of Keller [11] as reported in [31], i.e., that Hertz's theory overestimates the compressive stress on paper in the calender nip. Moreover, the average stress estimated from the present model is found to be a function of the viscoelastic–plastic characteristics of the substrate, while Hertz's solution is insensitive to changes in the substrate parameters. Despite these deviations, both the present model and Hertz's solution are in agreement in
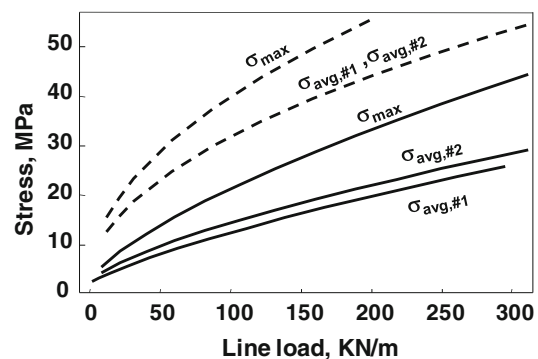
Fig. 4 Estimated maximum stress (σ_{max}) and average stress (σ_{avg}) based on the present model (*solid curves*) and Hertz' approximation (*dashed curves*) for paper #1 and paper #2
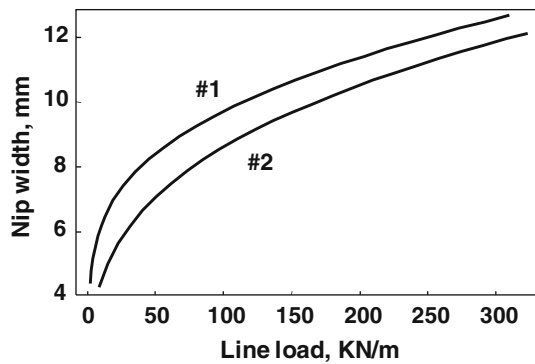
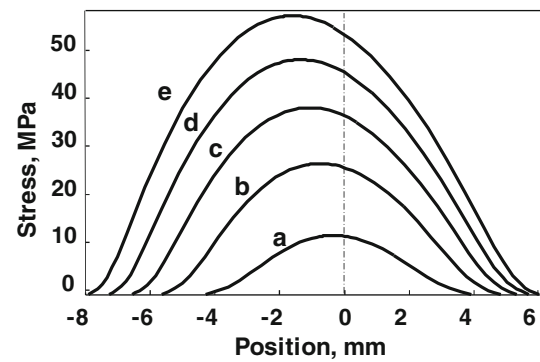Fig. 5 Predicted effect of line load on nip width for paper #1 and paper #2

Fig. 6 Compressive stress profiles under the nip for the soft-nip calendering of coated papers for various values of line load: (a) 50; (b) 150; (c) 250; (d) 350; and (e) 450 KN/m

predicting that the maximum stress for papers #1 and #2 are practically identical over the entire range of line load.

The observed change in the average stress with paper type is a reflection of the change in the nip width. Figure 5 demonstrates the relationship between nip width and the line load for papers #1 and #2. Based on this figure, for a typical line load of 250 KN/m, the predicted value for nip width is about 11 mm, which is comparable to the results reported elsewhere [16]. Furthermore, Fig. 5 shows that the nip width and the stress profile are affected by the characteristics of the paper substrate. Therefore, conventional static measurements commonly conducted in the absence of the paper substrate to estimate the nip width and stress profile can be misleading. In fact, it can be shown that the nip width will increase nearly linearly with the initial thickness of paper substrate. In other words, it is an over-simplification to ignore paper characteristics while evaluating the calendering process.

The predicted in-nip stress profiles qualitatively agree with the bell-shape profiles observed using pressure sensitive films in static compression experiments [15]. Similar results were also reported for dynamic compression experiments in the hard-nip calendering of paperboard [8]. Figure 6 illustrates the predicted stress profiles in the nip for the soft-nip calendering of paper #1 at different line loads. In this figure, the paper travels from left (negative coordinates) to right (positive coordinates). It appears that by increasing the line load, the peak stress shifts toward the nip entrance. This creates a larger increase in the ingoing nip width compared to the outgoing nip width, while maintaining the relatively symmetrical shape of the stress profile.

Cover thickness and modulus of elasticity

Perhaps the most important feature of soft-nip calendering is the effect of the soft cover material on the nip length and, hence, on the dwell time. A thicker and softer roll cover is expected to increase the nip length and hence decrease the maximum (and average) stress in the nip.

The maximum stress and the dwell time in the nip depend on the soft cover characteristics. By increasing the elastic modulus of the soft cover, the maximum compressive stress in the paper increases and asymptotically approaches the maximum stress in hard-nip calendering (Fig. 7a). In the meantime, by increasing the soft cover thickness, σ_{max} decreases to a plateau level that depends on the applied line load (Fig. 7b). Changes in the dwell time follow an opposite trend compared to the in-nip stress. Figure 7c and d shows the model predictions for typical values of roll cover thickness and modulus. The predicted dwell time at a line load of 300 kN/m is about 0.7 ms, which is similar to the values reported in literature [31]. As seen from this figure, decreasing the roll cover modulus and increasing its thickness result in a higher dwell time.

Roll diameter and calendering speed

A practical issue concerning the operation of calendering machines is addressing changes in the diameter and speed of calender rolls. Increasing calendering speed and reducing the calender roll diameter will reduce the dwell time of the coated paper. Therefore, in order to achieve the same level of permanent deformation, the line load has to be increased.

According to the Hertz theory, in order to achieve the same level of maximum compressive stress in soft-nip calenders made from the same material, the line load should increase proportionally to the effective roll diameter and calendering speed [16].

Based on Eqs. 14 and 5, to maintain the dwell time and maximum stress in the soft-nip calendering of paper, line load scales with the calendering speed, v, and square root of calender roll diameter, D. Hence, L should be chosen such that:
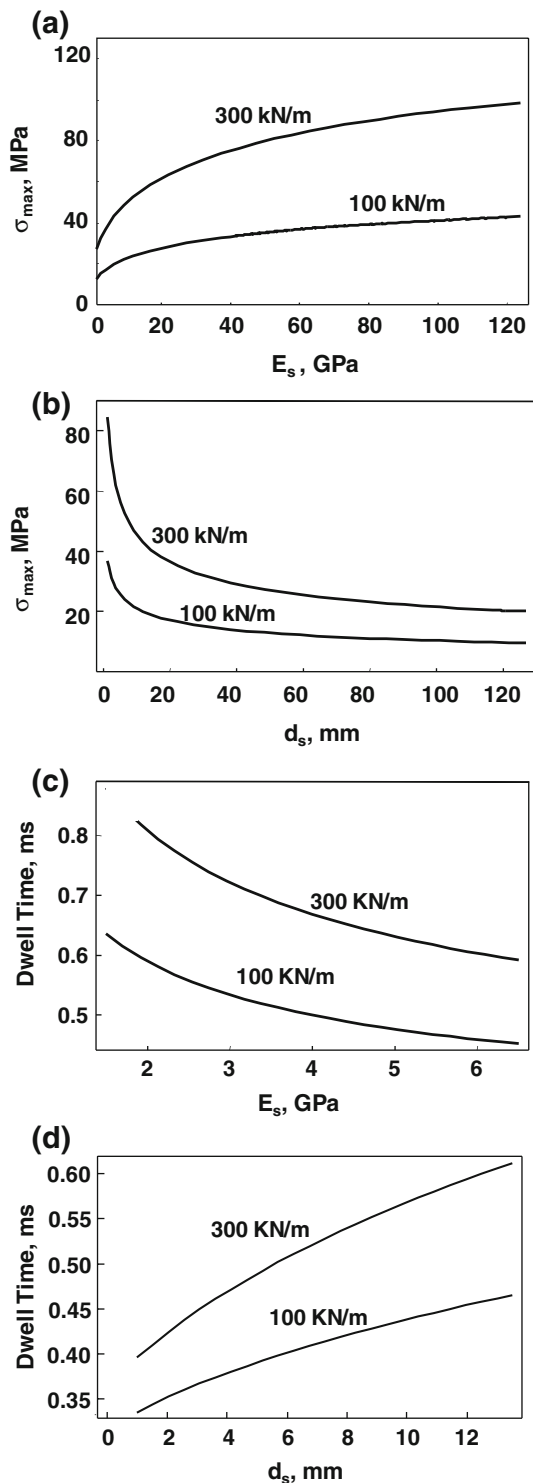
Fig. 7 Effect of soft cover elasticity, E_s, and thickness, d_s, on maximum compressive stress, σ_{max}, and dwell time for paper #1 at 100 and 300 KN/m line loads

$$\frac{L}{L_o} = \frac{v}{v_o} = \sqrt{\frac{D}{D_o}}. \tag{15}$$

This result is consistent with the nonlinear plastic deformation of a thin substrate in a hard rolling nip, proposed by Kerekes [12].

Paper compression in the nip

The transient response of paper in a calender nip can be divided into three stages: (1) the loading stage where the paper enters the nip and the compressive stress and strain in the paper increase from zero to their maximum levels under the applied line load; (2) the unloading stage where the applied stress and the compressive strain decrease until the paper exits the nip, and; (3) the relaxation stage where paper thickness continues to increase outside the nip and eventually reaches its final value. Figure 8a and b shows the predicted deformation of a coated paper undergoing soft-nip calendering with two different soft cover materials with elastic moduli of 6.0 and 1.5 GPa, respectively. The base sheet parameters are similar to those of paper #1 and the final paper thickness is 77 μm in both cases. Clearly, the elasticity of the soft cover material has a great impact on the strain history of paper in the calendering process. A stiffer cover material results in a shorter dwell time and nip length.

To better illustrate the dynamics of paper compression in the nip, the strain profiles for base paper and coating layers
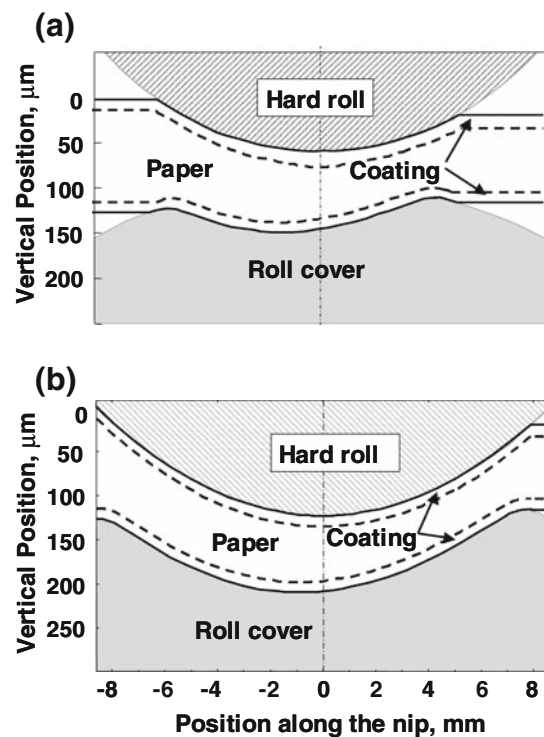

Fig. 8 Deformation of coated paper in soft-nip calendering for cover materials with: **a** high stiffness ($E_s = 6$ GPa), and; **b** low stiffness ($E_s = 1.5$ GPa). Line load: 250 KN/m, and base sheet: paper #1
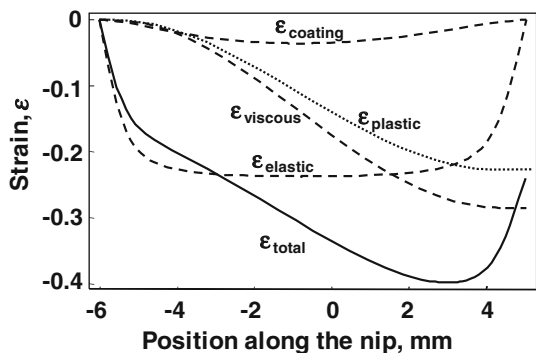
Fig. 9 Strain profiles for soft calendering of coated paper. Soft cover stiffness: 6 GPa, line load: 250 KN/m, and base sheet: paper #1
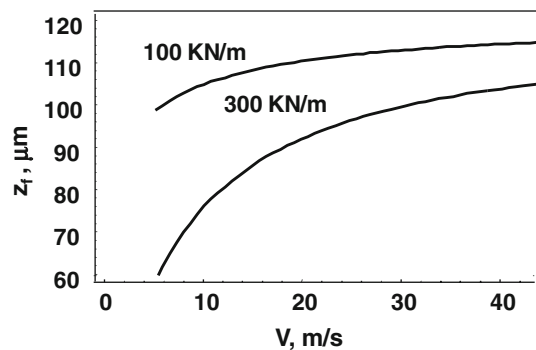

Fig. 10 Influence of calendering speed on the final thickness of paper substrate, z_f, at two values of line load (100 and 300 KN/m) for paper #1; initial thickness of substrate is 127 μm

Table 3 Paper characteristics and calendering data

	Hard nip	Soft nip
Grammage (g/m²)	45	
Initial thickness (μm)	80	
Speed (m/min)	820	820
Roll Temperature (°C)	80	80
Hard roll diameter (m)	0.430	0.750
Soft roll diameter (m)	–	0.530
Roll cover thickness (mm)	–	12
Roll cover hardness (Sh D)	–	92

Table 4 Experimental calendering data for the newsprint sample

Line load (KN/m)	Caliper (μm)	
	Hard nip	Soft nip
0	80	80
30	65	68
39	63	64
51	62	63
77	59	62

Table 5 Model parameters for the newsprint sample determined based on the hard-nip calendering data in Table 4

E_0 (MPa)	N_0 (−)	E_1 (MPa)	E_{20} (MPa)	η (kPa s)
43.9	0.02	61.9	13.6	4.8

are plotted in Fig. 9. This figure shows that the compressive strain and therefore the deformation of base paper in the nip is at least one order of magnitude larger than that of the coating layer. Therefore, the deformation of the coating layer has a minor effect on the final thickness of coated papers.

In the case of the calendering of coated papers, the permanent strain—or equivalently, the final thickness—of the coated paper is of practical interest. The final paper thickness depends on the processing speed and roll cover characteristics. For example, Fig. 10 shows the predicted effect of calendering speed on the final thickness of the paper. By increasing the speed, the final paper thickness increases and approaches a plateau. However, the level of this plateau depends on the applied line load, roll diameter, and the thickness and modulus of elasticity of the cover material.

Comparison with experimental data

Experimental data for the calendering of newsprint paper was provided by a calender machine manufacturer (Rheims, J., 2006, Private communication). Newsprint samples were calendered both in hard-nip (i.e., a hard roll against a hard roll) and soft-nip (i.e., a soft covered roll

against a hard roll) configurations, and the thickness of the paper at various line loads was recorded. The calendering conditions and the thickness-line load data are given in Tables 3 and 4. To examine the validity of the proposed model:

(1) Hard-calendering data were used to find the optimum model parameters for paper, i.e., E_i, N_i, E_1, E_{20}, η, and ε_∞, according to the procedure described elsewhere [14]. These parameters are given in Table 5.

(2) The above optimum model parameters were then used to predict the thickness-line load relationship for the sample in soft-nip calendering.

The predicted line load-thickness relationship for soft-nip calendering is given in Fig. 11. This figure shows that the model predictions are in close agreement with the experimental data.

Conclusions

A material model was developed for the deformation of coated substrates in a soft-rolling nip. This model was used
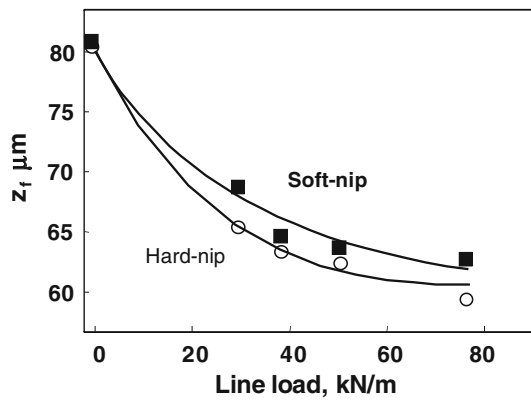
Fig. 11 Comparison between experimental data for final paper thickness (*symbols*) and predictions of the model developed in this work (*solid lines*). Hard-nip calendering: *solid circles*, and soft nip: *squares*

to simulate the compression of coated paper as a function of soft-nip calendering conditions. The predicted maximum compressive stress exerted on paper was found to be independent of the substrate characteristics over a wide range of line loads. However, both the nip width and the average compressive stress were a function of the paper parameters. This result indicates that the conventional static experiments conducted in the absence of a substrate to estimate nip width and stress profile can be misleading. This parametric study also revealed that the deformation of the coating layer had a negligible effect on the final thickness of the coated paper after calendering. According to this model, to maintain the same dwell time and maximum stress in the soft-nip calendering of coated (or uncoated) papers, line load should be scaled up proportionally to the calendering speed and the square root of the calender roll diameter, i.e., $L \propto v \propto \sqrt{D}$. Comparison with experimental data shows that the final thickness of paper was predicted accurately using the proposed model.

Appendix 1

Stack element strain function, ε, depends on the dimensions of the intersection zone of the calendar rolls, and is determined as a function of the position of the element along the nip. From Fig. 2, the relationship between ingoing nip length, a, and the value of maximum stack compression, c, can be found by solving the following set of equations:

$$x^2 + (z - r_1 \cos \phi_1)^2 = r_1^2$$
$$x^2 + (z + r_2 \cos \theta_1)^2 = r_2^2$$
$$c = r_1(1 - \cos \phi_1) + r_2(1 - \cos \theta_1) \qquad (16)$$
$$a = r_1 \sin \phi_1$$
$$r_1 \sin \phi_1 = r_2 \sin \theta_1$$

Coordinates x and z, and other variables in these equations are defined in Fig. 2. The first two equations in 16 describe the circumference of calender rolls, having their centers on the z-axis at the points $z_1 = r_1 \cos \phi_1$ and $z_2 = -r_2 \cos \theta_1$. The third equation is an expression for the maximum compression, and the last two expressions are for the ingoing nip width, a. Solution of this system of equations leads to an exact expression for the ingoing nip width as a function of the maximum stack compression, c:

$$a = \sqrt{2cr} \frac{\sqrt{\left(1 - \frac{c}{2r} + \frac{c^2}{4r(r_1+r_2)}\right)\left(1 - \frac{c}{2(r_1+r_2)}\right)}}{\sqrt{1 - \frac{c}{r_1+r_2}}}, \qquad (17)$$

where $r = r_1 r_2 / (r_1 + r_2)$. Considering that $c \ll r$ (or r_1, or r_2), Eq. 17 can be simplified to the well-known equation for the hard-nip calendering of paper [5]:

$$c \approx \frac{a^2}{2r}. \qquad (18)$$

Strain of the stack increases from zero to its maximum value, depending on its position along the nip. The change in stack thickness in the radial direction, dr, is equal to the distance BB''. The coordinates of B'' can be determined by solving the following system of equations:

$$x^2 + (z - r_1 \cos \phi_1)^2 = r_1^2$$
$$z = (r_2 \cos \theta / x_B)x - r_2 \cos \theta_1, \qquad (19)$$

where x_B is the position of the stack element along the x-axis that is represented by point B'. Therefore, the radial deflection of the stack can be found by subtracting $O_2 B'$ from the radius, r_2 (Fig. 2):

$$dr = r_2 - \sqrt{(r_2 \cos \phi_2 + z_{B''})^2 + x_{B''}^2}, \qquad (20)$$

where $x_{B''}$ and $z_{B''}$ are coordinates of point B''. Using the Taylor expansion and by ignoring higher order terms, the following expression for dr as a function of dimensionless time, $\tau (=x/a)$, is obtained:

$$dr \approx c\left(1 - \tau^2\left[1 + c\left(\frac{1}{r_2} - \frac{3}{r_1+r_2}\right)\right]\right). \qquad (21)$$

For commercial calenders, the ratio of c to roll radius is of the order of 10^{-3}. Therefore, the value of the expression in square brackets can be considered as unity, resulting in the distribution of stack deflection under the nip being expressed as a parabolic function of the dimensionless

time, τ. For comparison, change in the stack height in the vertical direction, dz, as a function of x, is:

$$dz = c - \left(r_1 - \sqrt{r_1^2 - x_{B''}^2}\right) - \left(r_2 - \sqrt{r_2^2 - x_{B''}^2}\right). \quad (22)$$

Using Taylor expansion and retaining two terms in the series in terms of x, and taking into account Eq. 18 for the nip width, an equation similar to (21) is obtained:

$$dz = c(1 - \tau^2). \quad (23)$$

Appendix 2

To illustrate the approach taken in this study, details for the determination of the stress function in the stack element for a simple case with constant elastic modulus of base paper and in the absence of coating layer (i.e., $N_i = 0$; $\beta = 0$) are shown below. The corresponding system of algebraic and differential equations is:

$$
\begin{aligned}
&\varepsilon_0(t) = \sigma(t)/E_0, \\
&\varepsilon_0'(t) = \sigma'(t)/E_0, \\
&E_{12}\varepsilon_{12}(t) + \eta_p\varepsilon_{12}'(t) = \sigma(t), \\
&\varepsilon_{sE}(t) = \sigma(t)/E_s, \\
&\varepsilon_{sE}'(t) = \sigma(t)'/E_s, \\
&\eta_s\varepsilon_{s\eta}'(t) = \sigma(t), \\
&(1 - \alpha)\varepsilon_s(t) + \alpha\varepsilon_p(t) = \varepsilon(t), \\
&(1 - \alpha)\varepsilon_s'(t) + \alpha\varepsilon_p'(t) = \varepsilon'(t), \\
&\varepsilon_p(t) = \varepsilon_0(t) + \varepsilon_{12}(t), \\
&\varepsilon_p'(t) = \varepsilon_0'(t) + \varepsilon_{12}'(t), \\
&\varepsilon_s(t) = \varepsilon_{sE}(t) + \varepsilon_{s\eta}(t), \\
&\varepsilon_s'(t) = \varepsilon_{sE}'(t) + \varepsilon_{s\eta}'(t).
\end{aligned}
\quad (24)
$$

In the above equations, ε is the total strain in the stack element, and ε_o, ε_{12}, ε_{sE}, $\varepsilon_{s\eta}$ represent strain in elements E_o, η_p, E_s, and η_s. Finally, ε_s and ε_p represent the strain in the paper and in the soft cover.

To derive the differential equations for the stress function, the above system of equations (24) is first solved for paper strain $\varepsilon_p(t)$ and its time derivative in terms of the stress function, $\sigma(t)$:

$$
\begin{aligned}
\varepsilon_p(t) =& \frac{\sigma(t)}{E_0} \\
&+ \frac{\alpha\eta_s\sigma(t) + \eta_p\left(-\eta_s\varepsilon'(t) + \frac{\alpha\eta_s\sigma'(t)}{E_0} + (1-\alpha)\left(\sigma(t) + \frac{\eta_s\sigma'(t)}{E_s}\right)\right)}{aE_{12}\eta_s}, \\
\varepsilon_p'(t) =& \frac{E_s\sigma(t) + \alpha E_s\sigma(t) + E_s\eta_s\varepsilon'(t) - \eta_s\sigma'(t) + \alpha\eta_s\sigma'(t)}{\alpha E_s\eta_s}.
\end{aligned}
\quad (25)
$$

By differentiating the first equation and equating it with the second one, we obtain:

$$
\begin{aligned}
&\sigma(t) + \left(\frac{\eta_p}{E_{12}} + \frac{\alpha(E_0 + E_{12})\eta_s}{(1-\alpha)E_0 E_{12}} + \frac{\eta_s}{E_s}\right)\sigma'(t) \\
&+ \left(\frac{\alpha E_s}{(1-\alpha)E_0} + 1\right)\frac{\eta_p\eta_s}{E_{12}E_s}\sigma''(t) \\
&= \frac{\eta_p\eta_s\varepsilon''(t)}{(1-\alpha)E_{12}} + \frac{\eta_s\varepsilon'(t)}{(1-\alpha)}.
\end{aligned}
\quad (26)
$$

Furthermore, if the soft cover thickness approaches zero, or if $\alpha \to 1$, this equation will describe stress distribution in the hard-nip calendering of paper. Alternatively, when $\alpha \to 0$, the equation is transformed to the Maxwell's equation for the roll cover.

Boundary conditions for $\sigma(t)$, corresponding to the point of the first contact of paper with hard roll at time "$-t_1$", are determined from the expression for $\varepsilon_p(t)$ (Eq. 25) knowing that $\varepsilon_s(-t_1) = 0$, $\varepsilon_p(-t_1) = 0$, and can be written in the following form:

$$
\begin{aligned}
&\sigma(-t_1) = 0, \\
&\sigma'(-t_1) = E_s\varepsilon'(-t_1).
\end{aligned}
\quad (27)
$$

This differential equation can be rewritten in a short form by introducing the differential operator $L[\ldots]$ for definition of the left-hand side of the equation:

$$
\begin{aligned}
L[\sigma] =& \sigma + \sigma'\left(T_s + T_p + \frac{\alpha E_s}{(1-\alpha)H}T_s\right) \\
&+ \sigma''T_s T_p\left(1 + \frac{\alpha E_s}{(1-\alpha)E_0}\right),
\end{aligned}
\quad (28)
$$

where $T_p = \eta_p/E_{12}$, $T_s = \eta_s/E_s$, $H = E_o E_{12}/(E_o + E_{12})$. Hence, the differential equation for the stress function has the following form:

$$L[\sigma] = (\varepsilon''(t)T_p + \varepsilon'(t))\frac{T_s E_s}{(1-\alpha)}. \quad (29)$$

Using a similar procedure, a differential equation for the viscous deformation of the paper and roll cover can be derived:

$$
\begin{aligned}
&L[\varepsilon_p] = \left(\varepsilon'(t) + \varepsilon''(t)\frac{HT_p}{E_0}\right)\frac{T_s E_s}{(1-\alpha)H}, \\
&\varepsilon_p'(-t_1) = \frac{E_s\varepsilon'(-t_1)}{E_0 - \alpha E_0 + \alpha E_s}, \\
&L[\varepsilon_{s\eta}] = \frac{\varepsilon(t) + T_p\varepsilon'(t)}{\alpha - 1}, \\
&\varepsilon_{s\eta}(-t_1) = 0, \\
&\varepsilon_{s\eta}'(-t_1) = 0.
\end{aligned}
\quad (30)
$$

Here, $L[\ldots]$ is the differential operator defined by Eq. 28.

References

1. Azadi P, Farnood R, Yan N (2008) J Comput Mater Sci 42:50
2. Azadi P, Nunnari S, Farnood R, Kortschot MT, Yan N (2009) Prog Org Coat 64:356
3. Bharwadj S, Kortschot M, Farnood R (2006) J Pulp Pap Sci 32:201
4. Browne TC, Crotogino RH (2001) In: Baker CF (ed) Proceedings of 12th fundamental research symposium held in Oxford. The Pulp and Paper Fundamental Research Society, pp 1001–1036
5. Browne TC, Crotogino RH, Douglas WJM (1996) J Pulp Pap Sci 22:170–173
6. Crotogino RH (1980) Trans Tech Sec 6:TR89
7. Feygin VB (1989) Treatment of paper under pressure at finishing process. Forest Industry, Moscow, Russia
8. Feygin VB (1999) Tappi J 82:183
9. Gerspach A (1993) Wochenblatt fuer Papierfabrikation 121:78
10. Harrysson A, Ristinmaa M (2008) Int J Solids Struct 45:3334
11. Keller SF (1991) J Pulp Pap Sci 18:89
12. Kerekes RJ (1976) Trans Tech Sec 2:88
13. Kwong K, Farnood R (2007) J Pulp Pap Sci 33:1
14. Litvinov V, Farnood R (2006) Nordic Pulp Pap Res J 21:365
15. Luong C, Lindem P (1997) Nordic Pulp Pap Res J 12:207
16. Lyons AV, Thuren AR (1994) Tappi J 75:95
17. Pawlak JJ, Keller DS (2005) Mech Mater 37:1132
18. Peel JD (1999) Paper science and paper manufacture. Angus Wilde Publications Inc., Bellingham, WA
19. Popil R (1989) In: Baker CF (ed) Transactions of the fundamental research symposium, vol 2. Mechanical Engineering Publications Ltd., London, UK
20. Provatas N, Uesaka T (2003) J Pulp Pap Sci 29:332
21. Qi D (1997) Tappi J 80:121
22. Rättö P (2002) Nordic Pulp Pap Res J 17:130
23. Rodal JJA (1989) Tappi J 72:177
24. Rodal JJA (1993) Tappi J 76:63
25. Saliklis E, Kuskowski S (1998) Tappi J 81:111
26. Stenberg N (2003) Int J Solids Struct 40:7483
27. Ting T, Johnston R, Chiu W (2000) Appita J 5:379
28. Vuoristo T, Kuokkala V, Keskinen E (2002) Key Eng Mater 221–222:221
29. Vuoristo T, Kuokkala V, Keskinen E (2000) Comp A Appl Sci Manuf 31:815
30. Wikström M, Nylund T, Rigdahl M (1997) Nordic Pulp Pap Res J 12:289
31. Wikström M, Rigdahl M, Steffner O (1996) J Mater Sci 31:3159. doi:10.1007/BF00354662